2.1 CHARACTERIZATION OF PROCESSING INDUCED IMPURITY PHASE PRECIPITATES IN THE AS-PROCESSED FCRD-NFA-1 —

S. Pal, M. E. Alam and G. R. Odette (UCSB), S. Maloy (LANL), D. Hoelzer (ORNL)

OBJECTIVE

This study is aimed at characterizing the microstructure and chemistry of the impurity phase precipitates produced in the as-processed NFA-1 alloy and determining their corresponding effect on mechanical properties.

SUMMARY

The NFA-1 contains detrimental impurity phases along with the desirable nano-oxides (NOs). The impurity phase precipitate particles appear as black, nearly round features in SEM micrographs, with a size distribution between 10 and 260 nm. The impurity particles are arranged as stringers in the direction of primary deformations during hot extrusion, and cross-rolling. Chemical analysis using electron probe micro-analyzer demonstrates that these particles are either rich in Ti or Y. TEM shows these features are primarily formed on grain boundaries and triple junction. The EDS shows that the particles are primarily Ti-O and fewer Y-O phases. Heat treatment at 1300°C/5 hr shows the complete dissolution of these particles, suggesting they are a metastable phase. The precipitates act as nucleation sites for ductile fracture at high temperature, reducing tensile ductility and fracture toughness.

PROGRESS AND STATUS

Introduction

Nanostructured ferritic alloys (NFAs) are designed in such a manner to contain 1-3 nm fine dispersions of Y-Ti–O nano-oxides to achieve both a high radiation tolerance by managing helium, and exceptionally high thermal stability up to ~1000°C [1-3]. The alloy also possesses a very high tensile strength and high temperature creep strength [1, 3]. It has been postulated that the excellent creep and radiation tolerance of this alloy is due to the presence of these fine scale nano oxides, which impede dislocation and boundary movements during high-temperature deformation. On the other hand, they can effectively trap helium in nanometer scale bubbles and prevents the formation of large voids [1, 2]. An enormous effort has been put forward to characterize the structure and chemistry of these nano-oxides using different characterizations techniques, such as TEM, APT, SANS, SAXS [4, 5]. However, microstructural characterization also reveals that the alloy consists of some larger sized precipitates 10-150 nm, rich in either Ti or Y [6, 7]. Chemical analysis of these precipitates using EDS and EELS suggest that they are composed of Ti-C-O-N or sometimes pure Y_2O_3, originating as a processing-induced inhomogeneity [1, 6, 7]. A little effort has been given to characterize the exact structure and chemistry of these precipitates, as well as its role on determining the mechanical properties of this alloy. The present investigation is a prelude towards that path.

Materials

The present investigation was carried out on a newly develop NFA alloy, FCRD-NFA-1, a variant of ODS class of steel. This alloy has been developed with a close collaboration between UCSB, LANL, and ORNL. The nominal composition of the alloy is 14Cr-3W-0.4Ti-0.3Y and balance Fe. The alloy powder is first ball milled, then canned and degassed at 400°C, and hot extruded (HE) at 850°C, which is further annealed for 1 hr and cross-rolled perpendicular to the HE direction, both at 1000°C. Microstructural characterizations were carried out using SEM and TEM. The elemental chemical analysis was performed using an electron probe micro-analyzer (EPMA) and an energy dispersive spectroscopy attachment on a TEM. Thin TEM lamellas are prepared using FIB lift-out methods. In order to characterize the thermal stability of the impurity phase precipitates, as-processed alloy sample were annealed at 1300°C for 5 hr inside a vacuum furnace.

Results

Figure 1b shows a representative SEM micrograph of the side surface (LS) of NFA-1 plate, where the grains are elongated in the extrusion direction. The impurity phase precipitates appear as black particle-like features, and collectively those are arranged as strings along the extrusion direction. The particles appear as near circular shaped. Size distribution and the average spacing between two particles, measured from the SEM micrographs of the top, side and front surfaces, are listed in Table 1.

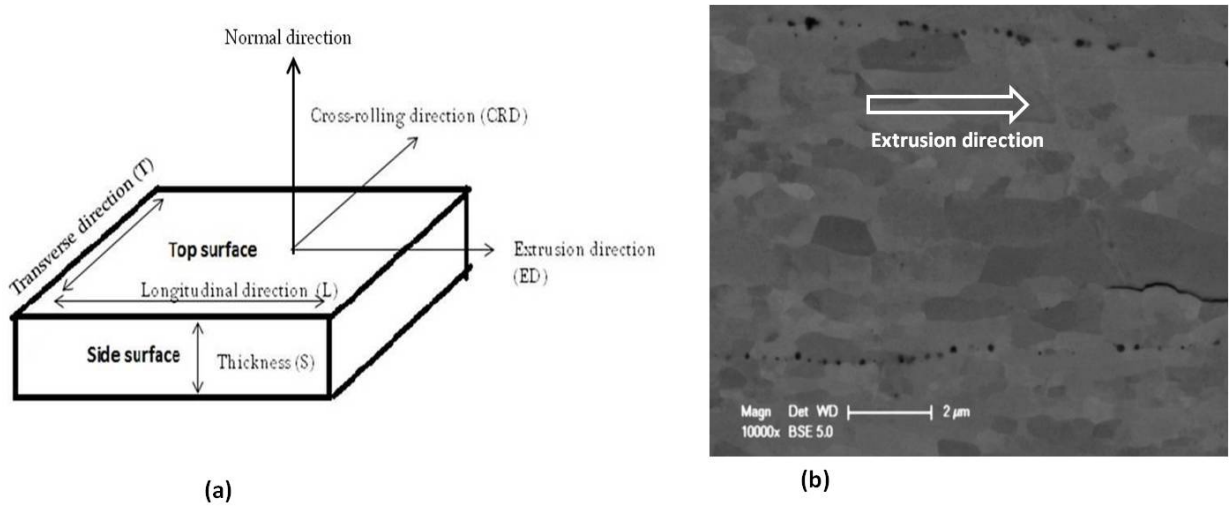

Figure 1. (a) A schematic of the NFA-1 plate showing longitudinal (L), transverse (T) and short thickness (S) directions. Planes parallel to the side surface is defined as LS, parallel to the top LT and parallel to the front face as TS. Extrusion and cross-rolling of the plate was carried out along the L and T direction as marked accordingly. (b) SEM micrographs of the LS view or plane parallel to the top surface of NFA-1 as processed plate shows impurity phase precipitates as a black particle like feature. Extrusion direction is marked with a white arrow.

Table 1. Statistics of particles size and interparticle spacing for planes parallel to the top (LT), side (LS) and front (TS) of as-processed NFA-1 plate.

Sample Orientation	Ti/Y rich particle size (nm)	Interparticle spacing along x (nm)
LT/ Top surface	57 ± 33 Range: 10-262	228 ± 106
LS/Side surface	62 ± 32 Range: 11-188	303 ± 210
TS/ Front surface	68 ± 33 Range: 22-180	279 ± 160

Figure 2a-f and Figure 3a-f display the compositional maps of the plane parallel to the side (LS) and top (LT) surfaces of the NFA-1 plate, measured using an electron probe micro analyzer. The Fe, Cr, and W are homogeneously distributed throughout the map; whereas, Ti and Y form clusters. The SEM micrographs together with EPMA maps confirm that those precipitates are rich in Ti and Y. The numbers of Ti-rich features far exceed Y rich particles.

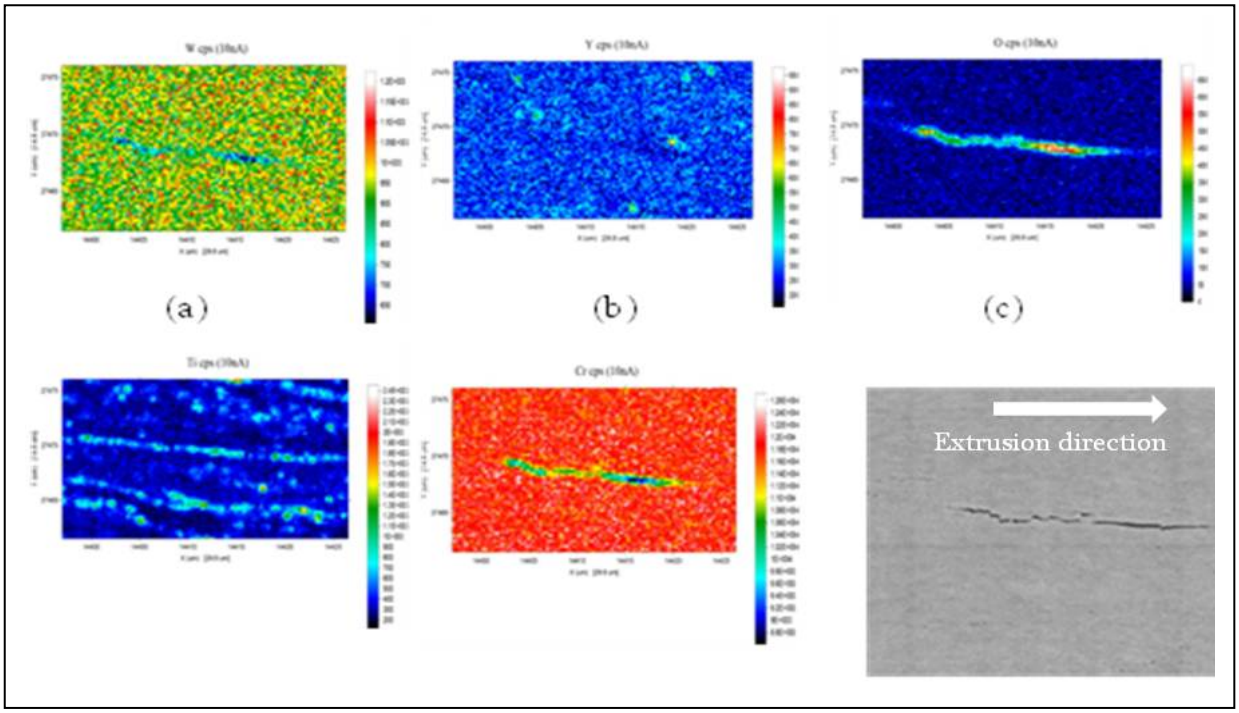

Figure 2. a-e) Elemental compositional maps for the LS view, and f) the cracked region of interest.

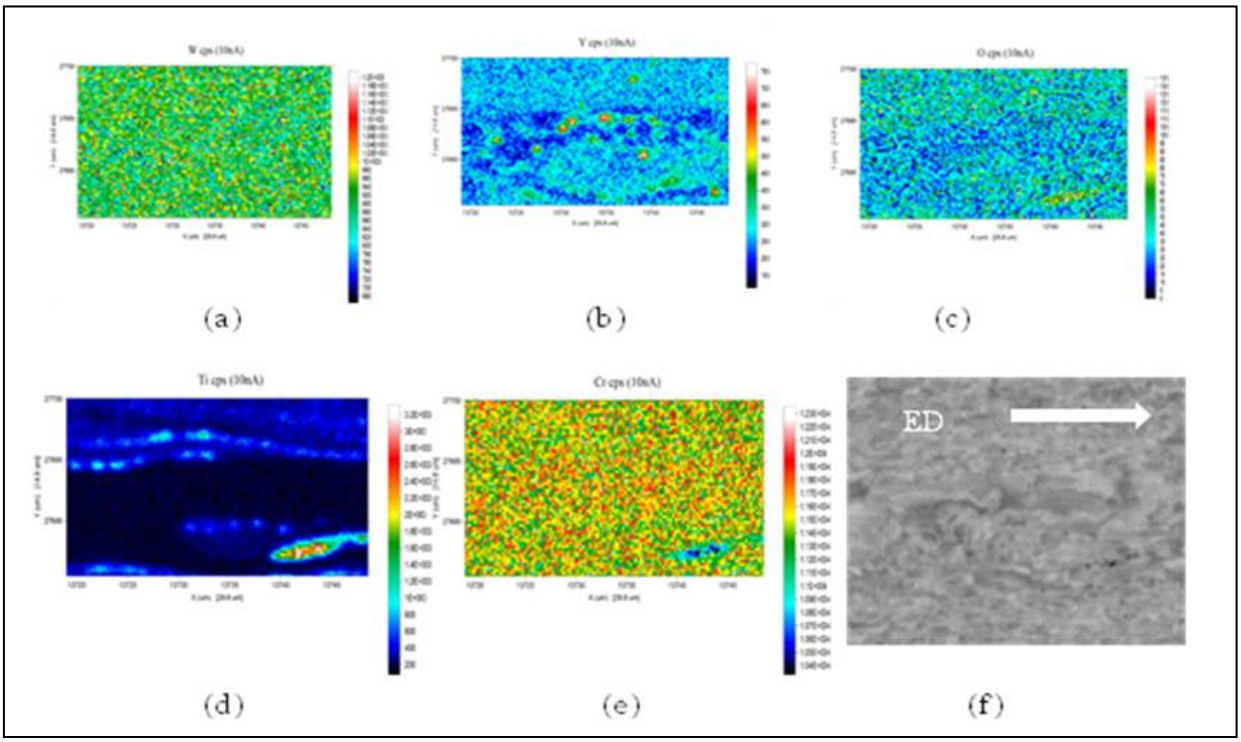

Figure 3. a-e) Elemental compositional maps for the LT view, and f) the region of interest.

An in-depth microstructural characterization and chemical analysis of these impurity phase precipitates were performed using TEM. Similar to SEM micrographs, these precipitates are also appeared as dark particle-like features in an STEM-HAADF image (Figure 4). The BF-TEM images of two of these precipitates are shown in Figure 5a and Figure 5b. From the micrographs, it is clearly evident that those precipitates are nucleated at either grain boundary or grain boundary triple junction. Both the precipitates have a size of ~ 50 nm.

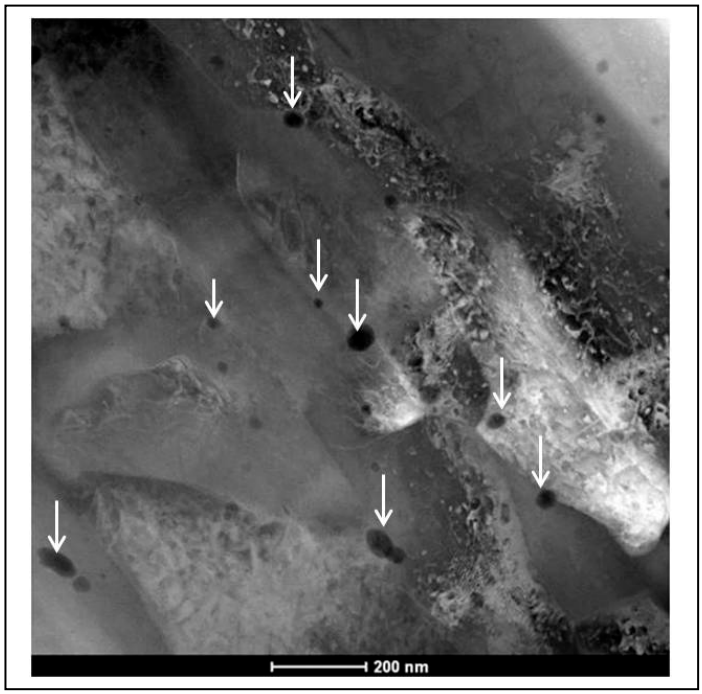

Figure 4. STEM–HAADF image of the NFA-1 alloy shows impurity phase precipitates as black particles.

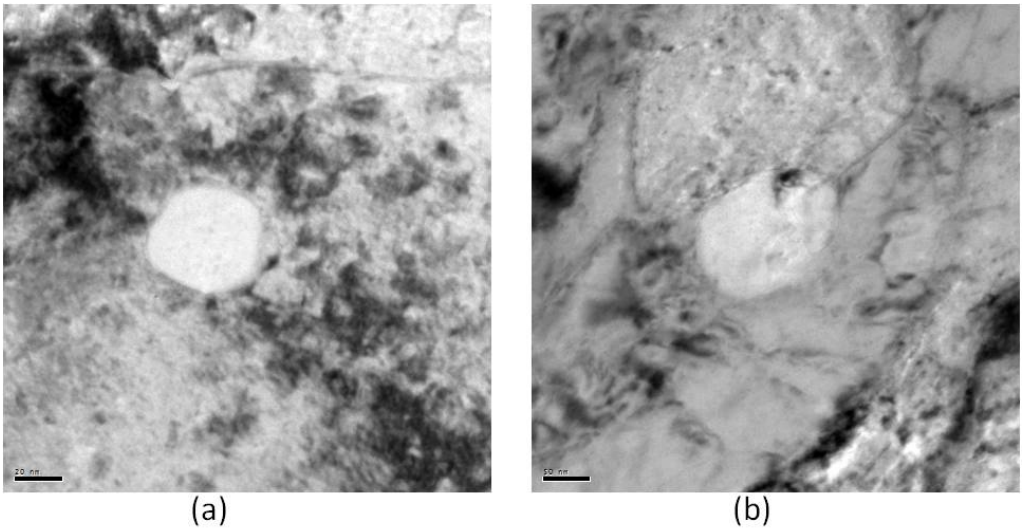

Figure 5. a), and b) BF-TEM image of an impurity phase precipitate nucleated at a grain boundary and triple junction, respectively.

Lattice fringe image of the precipitate, shown in Figure 6a, clearly displays that the interface between the matrix and precipitate is completely incoherent. The shape of the precipitate is not spherical; rather it takes a faceted polyhedral shape. The Fast Fourier Transform (FFT) pattern of the precipitate captured from the region, marked as 2, displays that the precipitate has a different structure than NOs of $Y_2Ti_2O_7$ or $Y_2Ti_2O_5$, seen in Figure 6b [5]. The amorphous-like appearance of the region, marked as 1, implies that this portion of the precipitate does not satisfy a zone axis condition, whereas region 2 does satisfy a near zone axis condition. This gives an indication of strongly faceted nature of the precipitate. A higher magnification view of the lattice fringe, shown in Figure 7, does not exhibit continuous lattice fringes. Even within the precipitate, regions of discontinuous lattice fringes with a dark contrast are clearly visible. A STEM-HAADF image of the same particle also shows some white features inside the precipitates (Figure 8a). The EDS spectrum collected from the whole particle, shown in Figure 8b, indicates that this particle is enriched with Y and O.

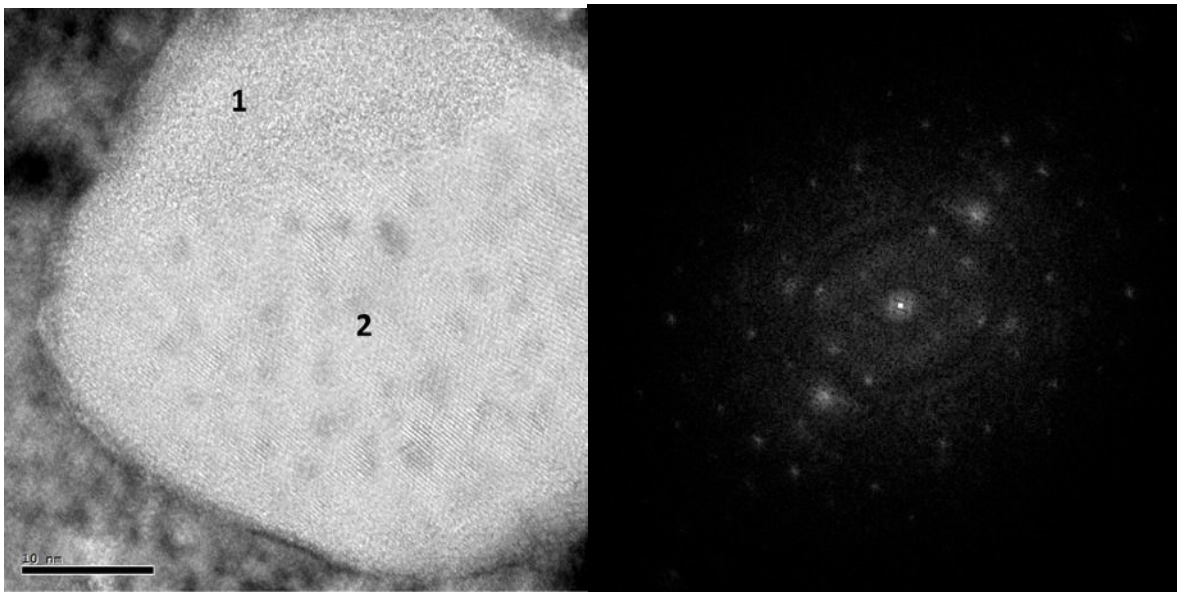

Figure 6. a) HR-TEM image of the precipitates shown in Figure 5a). b) FFT pattern of the PPT captured from the location, marked as 2 in Figure a).

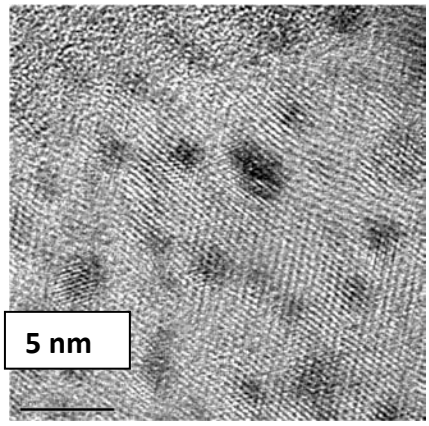

Figure 7. Higher magnification view of the lattice fringe image of the precipitates shown in Figure 5a.

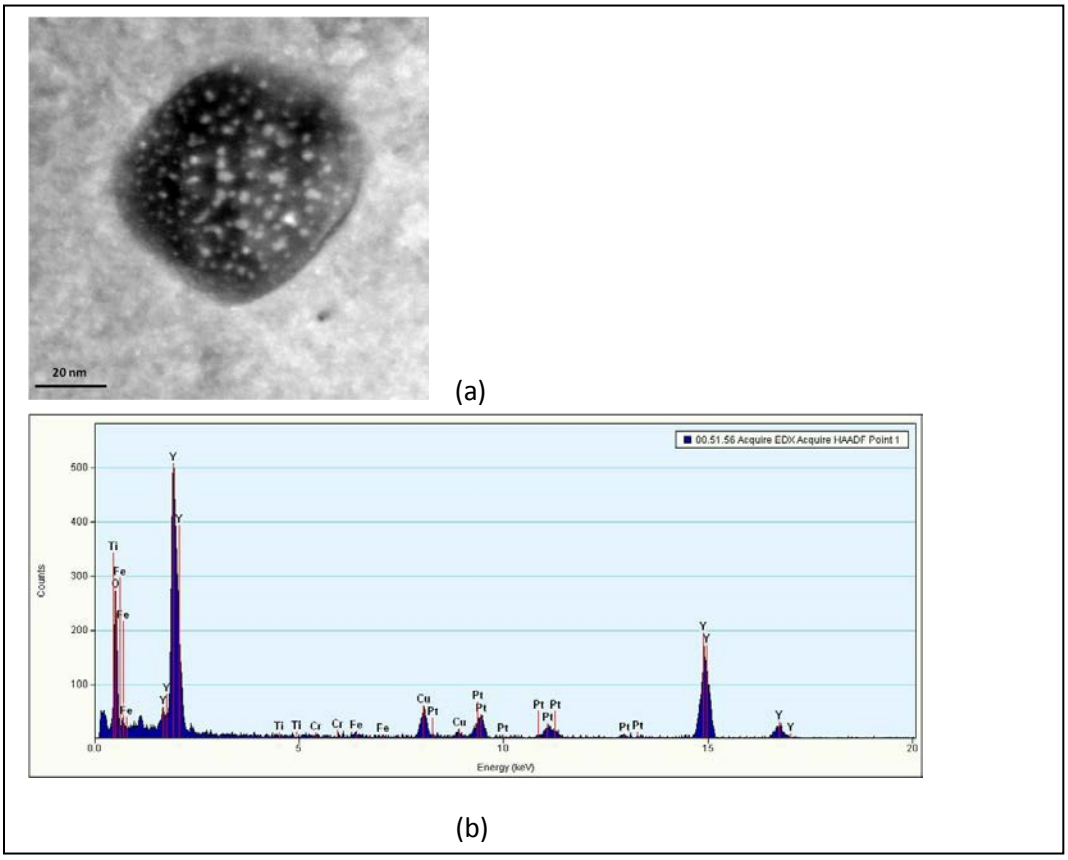

Figure 8. a) STEM-HAADF image of a Y-rich precipitates b) corresponding EDS spectrum of the whole particle.

The STEM–HAADF imaging coupled with an EDS line profile also shows that there are precipitates, which are rich in Ti (Figure 9). A dark contrast inside these precipitates has been observed, which shows higher oxygen concentration compared to the brighter portion of the precipitates. The Ti signal has an opposite trend compared to oxygen. Fe and Cr signal have not been detected.

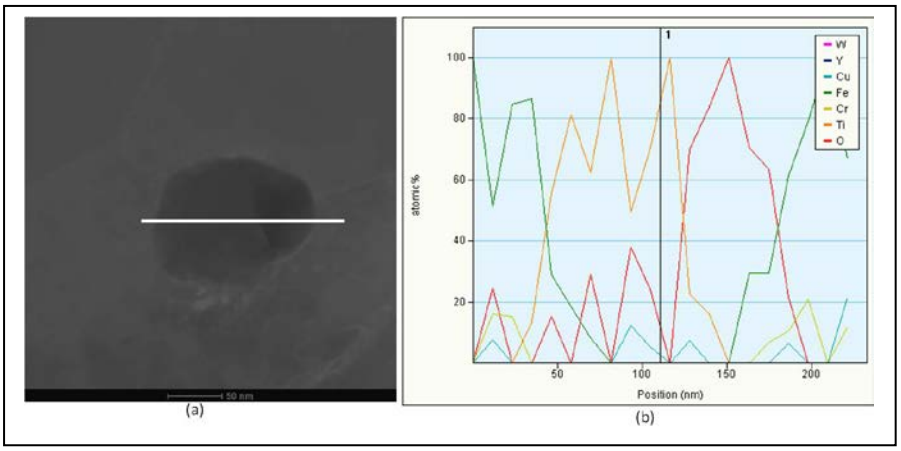

Figure 9. a) STEM-HAADF image of an impurity phase precipitates, b) corresponding EDS composition profiles of different elements present in the alloy, captured along the marked line in Figure 9a).

<u>The effect of high-temperature heat treatment on the impurity phase precipitates</u>:

Effect of high-temperature heat treatments on these precipitates is quite profound, and, it has been observed that these precipitates are not thermally stable. Figure 10a shows that the large precipitates do not even exist after a heat treatment of 1300°C for 5 hr.

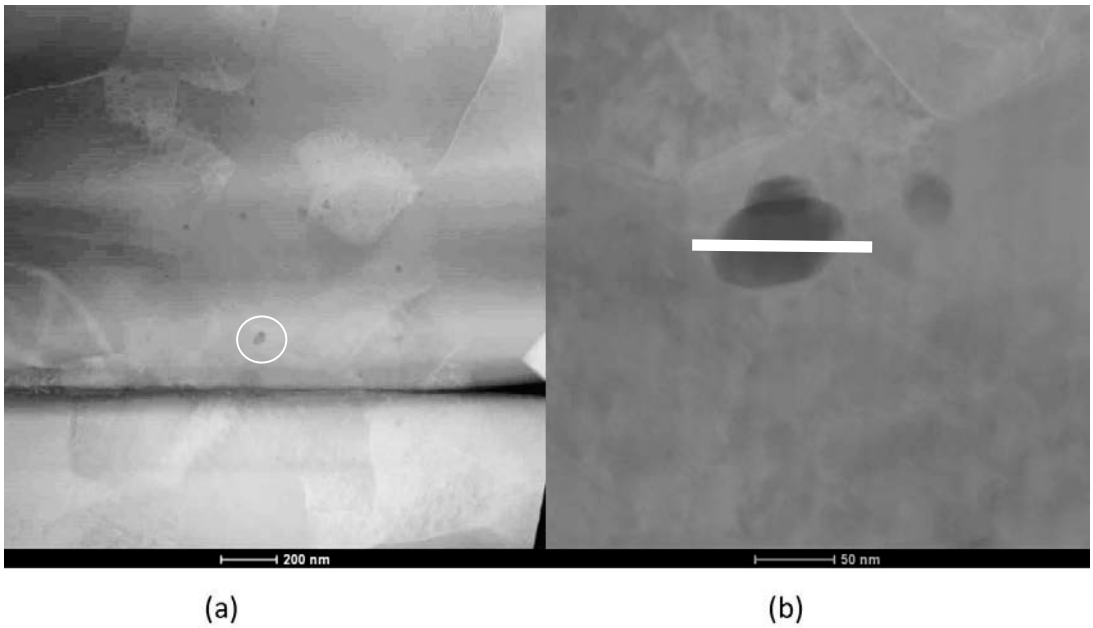

Figure 10. a) STEM-HAADF image of 1300°C/5 hr. heat treated sample. b) Magnified view of the precipitate marked in Figure 10a using a black circle.

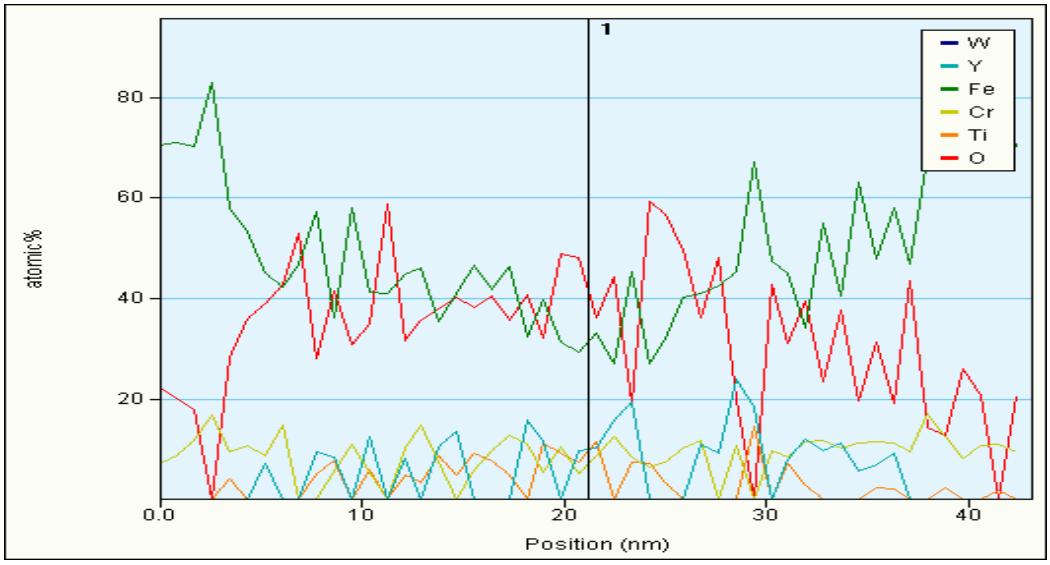

Figure 11. Composition profile of the different elements presents in the NFA alloy measured along the marked line in Figure 10b).

The EDS line profile analysis, shown in Figure 11, depicts that after heat treatments of 1300°C/5 hr, Ti and Y content of the precipitates are significantly reduced; whereas, in the as-processed condition precipitates are enriched with either Ti or Y, seen in Figure 7 and Figure 8b. The measured average ratio of Y, Ti and O is ~ 1/1/3.5. This suggests that the imaged precipitate is not the same impurity phase precipitate; rather, it is a nano-oxide of $Y_2Ti_2O_7$ which coarsens during the heat treatment. On one hand it is well known that growth kinetics of NOs are extremely sluggish, therefore coarsening of a NOs up to a size of ~ 60 nm (ure 11b), is extremely difficult for the present heat treatment conditions [1]; rather, it is more probable for the precipitates to transform into NOs. Figure 11b also shows that inside NOs significant amounts of Fe and Cr coexist, suggesting a core-shell kind of structure. This kind of core-shell kind of structure of NOs is also reported by other researchers [6, 7]. Though the kinetics of dissolution and thermal stability of the impurity phase precipitates has not been understood properly; experimental evidence suggests these impurity phase precipitates are metastable. Surprisingly for the present instance, we have not found any of the impurity phase precipitates in 1300°C/5 hr annealed sample.

Effect of impurity precipitates on high-temperature tensile behavior:

Figure 12 shows the variation of yield strength with temperature for the FCRD-NFA-1 alloy, where test specimens were made from three different orientations of the plate top, side and front surfaces. The plots suggest that there might be two different mechanisms operative: one from room temperature to 400°C and another one above 400°C. A similar kind of dependence of fracture toughness of NFA alloys on temperature is also reported by Byun et.al [8]. At room temperature fracture of the alloy is controlled by mesoscopic features; whereas, above 200°C continuous reduction in the toughness is caused by the shallow plastic zone formation due to the nanostructure of the alloy itself. It was also observed that at 700°C fracture occurs through de-bonding of low toughness grain boundaries [8].

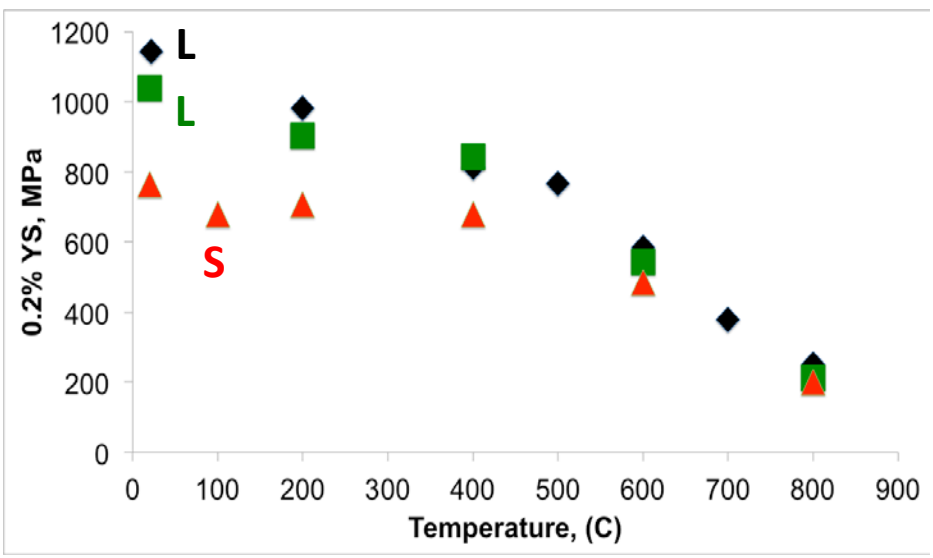

Figure 12. Yield strength of NFA-1 alloy tested at different temperatures.

Fractography of the 600°C tensile tested specimen clearly demonstrates that the failure of the alloy at elevated temperature occurs by ductile failure mode with dimple formation. A closer observation of the fracture surface (Figure 13a and Figure 13b) reveals that fracture processes at high temperature occur through de-bonding of the grain boundary, which initiates from those impurity phase precipitates. Notably, all these impurity phase precipitates are only observed at the grain boundaries and are incoherent in nature. This altogether suggests that this impurity phase precipitates have an important role on determining the high-temperature behavior of this alloy.

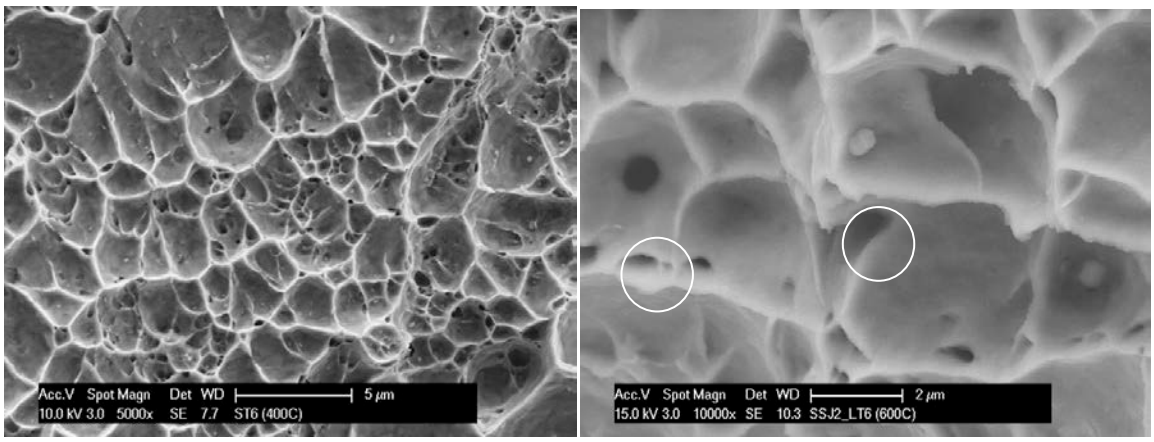

(a) (b)

Figure 13. a), and b) show the both low and high mag image of the fracture surface of a tensile sample tested at 600°C. Particles are marked using a white circle in Figure 13b).

SUMMARY

Experimental evidence clearly demonstrates that the large size precipitates are not same as the NOs, usually found in the NFA alloys. These precipitates are neither oxynitride nor oxycarbaide particles as previously reported [6, 7]. They are usually bigger in size and lesser in number compared to the NOs and they form only at the grain boundary. These precipitates are incoherent in nature and do not have any significant effect on the room temperature mechanical properties of these alloys; but decohesion of these precipitates during high-temperature deformation may degrade the high-temperature mechanical properties of the alloy.

Future Work

- Accurate determination of the chemistry and crystal structure of these precipitates will be performed using electron energy loss spectroscopy and convergent beam diffraction techniques.
- High-temperature mechanical properties of this alloy degrade through decohesion of these precipitates from grain boundary during deformation. Post-deformation TEM characterization of the grain boundary will also be performed on the high temperature tensile tested sample.

References

[1] G.R. Odette, “Recent Progress in Developing and Qualifying Nanostructured Ferritic Alloys for Advanced Fission and Fusion Applications”, JOM, 66 (2014) 2427-2441.
[2] G.R. Odette, “Recent Developments in Radiation resistant Steels” Annu. Rev. Mater. Res, 38 (2008) 471-503.
[3] M.C. Brandes, “Creep behavior and deformation mechanism in a nanoclustered strengthen ferritic steel” Acta Materialia, 60 (2012) 1827-1839.
[4] M. Ohnuma, “A new method for the quantitative analysis of the scale and composition of nanosized oxide in 9Cr-ODS steel” Acta Materialia, 57(2009), 5571-1839.
[5] Y. Wu, **“**Transmission electron microscopy characterization of the nanofeatures in nanostructured ferritic alloy MA957” Acta Materialia, 60(2012), 3456-3468.
[6] M.C.Brandes, “Morphology, structure, and chemistry of nanoclusters in a mechanically alloyed nanostructured ferritic steel” J.Mater. Sci, 47 (2012), 3913-3923.
[7] M.K. Miller, “Role of alloying elements in nanostructured ferritic steel” Material Science and Technology, 27 (2011) 729-734.
[8] TS Byun, “High-temperature fracture characteristics of a nanostructured ferritic alloy (NFA)” Journal of Nuclear Materials, 407 (2010) 78-82.